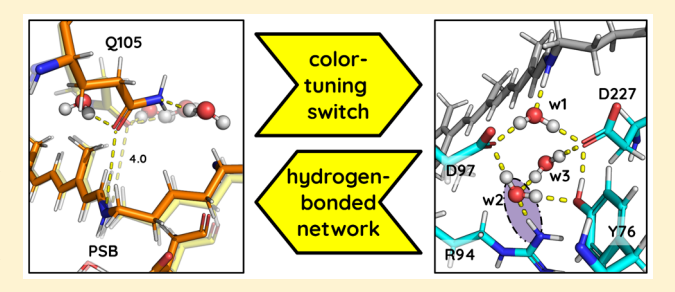


# Theoretical Insights into the Mechanism of Wavelength Regulation in Blue-Absorbing Proteorhodopsin

Choongkeun Lee,<sup>†</sup> Sivakumar Sekharan,<sup>†,§</sup> and Blake Mertz\*,<sup>†,‡</sup>

Supporting Information

**ABSTRACT:** Proteorhodopsin (PR) is a light-driven proton pump that is most notable for ushering in the discovery of an ever-increasing number of microbial retinal proteins that are at the forefront of fields such as optogenetics. Two variants, blue (BPR) and green (GPR) proteorhodopsin, have evolved to harvest light at different depths of the ocean. The color-tuning mechanism in PR is controlled by a single residue at position 105: in BPR it is a glutamine, whereas in GPR it is a leucine. Although the majority of studies on the spectral tuning mechanism in PR have focused on GPR, detailed under-



standing of the electronic environment responsible for spectral tuning in BPR is lacking. In this work, several BPR models were investigated using quantum mechanics/molecular mechanics (QM/MM) calculations to obtain fundamental insights into the color tuning mechanism of BPR. We find that the molecular mechanism of spectral tuning in BPR depends on two geometric parameters, the bond length alternation and the torsion angle deviation of the all-trans-retinyl chromophore. Both parameters are influenced by the strength of the hydrogen-bonded networks in the chromophore-binding pocket, which shows how BPR is different from other microbial rhodopsins.

#### INTRODUCTION

Proteorhodopsin (PR) is a membrane protein that functions as a light-harvesting proton pump, and it is ubiquitous throughout lower forms of life (e.g., marine planktonic bacteria, archaea, and eukaryotes. 1,2 Understanding the mechanism of PR function is of vital importance, as PR is intimately involved in the carbon cycle of marine ecosystems<sup>3</sup> and also shows promise in light-driven applications.<sup>4</sup> PR possesses a seven transmembrane helical (7TM) topology typical of retinal proteins.<sup>5</sup> Photoactivation is initiated when the covalently bound protonated Schiff base of the all-trans retinyl chromophore (PSB) absorbs a photon and undergoes an all-trans to 13-cis isomerization. This leads to large-scale conformational changes in the protein, which is then used to facilitate proton transport. The photocycle of PR results in the net transfer of a single proton across the inner membrane from the cytoplasm to the periplasm, generating a proton gradient that facilitates ATP synthesis (Figure 1).

PR has evolved into two variants that optimally absorb the available light in a marine environment, blue (490 nm, BPR) and green (525 nm, GPR) PR. 1,2 Color tuning between the variants is controlled by a single residue in the binding pocket: in BPR the residue is a glutamine (Q105), whereas in GPR it is a leucine (L105) (all subsequent residue numbers correspond to GPR numbering unless otherwise specified). This colortuning switch leads to structural differences within the retinal binding pocket. Most notable is that Q105 in BPR can form a hydrogen bond with the Schiff base (SB) linkage, leading to its characteristic blue-shifted absorption maximum ( $\lambda_{max}$ ) in the dark state (Figure 1).8,9

Although the photocycle of PR is similar to bacteriorhodopsin (bR), distinct differences exist between the two retinal proteins. The p $K_a$  of the proton acceptor in PR (D97, ~7.1) [6] is much higher than in bR (D85,  $\sim 2.5$ ), <sup>10</sup> allowing PR to act as a vectorial proton pump: at environmental (alkaline) pH, PR acts as an outward proton pump, but under acidic pH this direction is reversed and protons are pumped into the cell. 11 A key interaction that leads to this vectoriality is the presence of a histidine residue (H75) that is conserved in PR and many other recently discovered retinal proteins but is absent in bR (Figure S1). H75 stabilizes the p $K_a$  of D97 through a hydrogen-bonding interaction between the side chains of each residue. A recent solid-state NMR study further elucidated this relationship, showing that tautomerization of the proton on H75 plays a key role in stabilizing the M photointermediate. 12-14

Fundamental understanding of the photocycle of retinal proteins relies upon characterization of the arrangement of waters, the chromophore, and amino acid side chains within the binding pocket. Water molecules are essential to the

Received: August 28, 2019 Revised: November 22, 2019 Published: November 22, 2019

<sup>&</sup>lt;sup>†</sup>C. Eugene Bennett Department of Chemistry, West Virginia University, Morgantown, West Virginia 26506, United States

<sup>\*</sup>WVU Cancer Institute, West Virginia University, Morgantown, West Virginia 26506, United States

<sup>&</sup>lt;sup>§</sup>XtalPi Inc, 245 Main Street, 12th Floor, Cambridge, Massachusetts 01242, United States

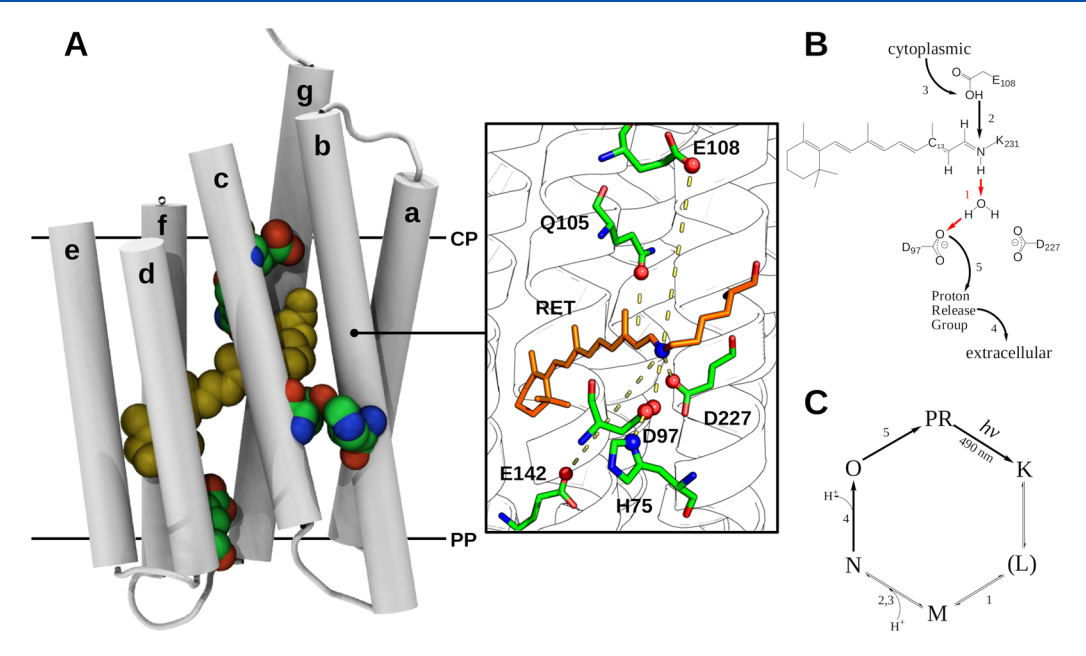
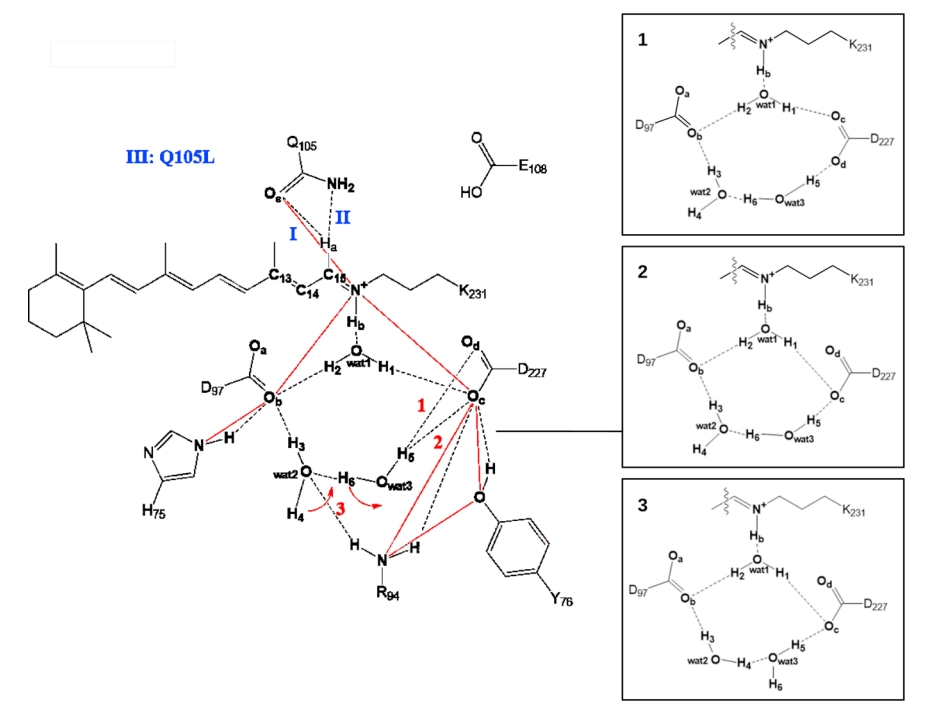


Figure 1. Active sites and schematic of photocycle of PR. (A) PR possesses a conserved heptahelical tertiary structure containing the covalently bound retinyl chromophore. The retinal binding pocket lies at the center of the protein and acts as a hub for the proton-pumping mechanism. Yellow: retinal; multicolored spheres: functionally important residues. CP: cytoplasmic; PP: periplasmic. Inset: close-up of important interactions between retinal the binding pocket of BPR. (B) Schematic of the residues implicated in the proton-pumping mechanism. D97: proton acceptor; E108: proton donor; D227: complex counterion; H75: stabilizes D97; and Q105: color-tuning residue. The initial activation step is photoisomerization (PR  $\rightarrow$  K states). Five proton transfers take place: (1) from Schiff base (SB) to D97, representing formation of the M state; (2) from E108 to SB (formation of N state); (3) regeneration of protonated E108 from bulk cytoplasm; (4) release of proton to the periplasm; and (5) from D97 to the proton release group. (C) Photocycle of proteorhodopsin. For each photointermediate, a unique hydrogen-bonded network and protonation state exists.

Scheme 1. Retinal Binding Pocket Conformations Tested in This Study<sup>a</sup>



"I:  $O_{\epsilon}$  of Q105 interacting with PSB. II: NH<sub>2</sub> of Q105 interacting with PSB. III: Q105L mutation, interacting with PSB. Sub-model 1: w1 interacting with both side chain carbonyl groups of D97 and D227. Sub-model 2: w1 interacting with keto group of D227. Sub-model 3: w2 fully hydrogen-bonded to the pentagonal water cluster in the binding pocket.

function of retinal proteins, 15 as they make it possible for protons to be transferred between the components involved in function (i.e, the proton donor, SB, proton acceptor, and

proton release group). The retinal binding pocket is characterized by the arrangement of a pentameric hydrogen-bonding network (HBN) between the SB, the proton acceptor

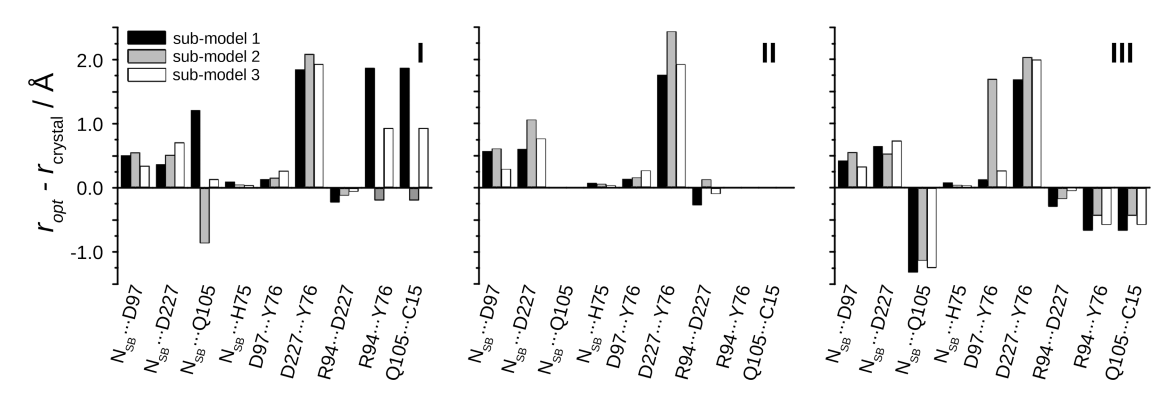


Figure 2. Key intramolecular interactions in BPR show that orientation of Q105 has a subtle effect on the retinal binding pocket and extracellular half-channel. Deviation of intramolecular distances  $(r_{\text{opt}})$  from corresponding distances in the X-ray crystal structure  $(r_{\text{crystal}})$  for all submodels in group I (left), group II (middle), and group III (right). (For complete data set, see Table S2 in the Supporting Information.)

and/or the counterions, and three water molecules. 16,17 When retinal proteins are dehydrated (i.e., disruption of the HBN), this alters their function, either through a spectral shift<sup>18</sup> or through deactivation of the protein. 9 Although a crystal structure of BPR was recently solved, 20 it lacked water molecules near the SB. In addition, previous spectroscopic studies indicated that the HBN within the PR retinal binding pocket is slightly different from that of bR.21 Therefore, characterization of the role of internal water molecules is necessary for the fundamental understanding of structurefunction relationships in PR.

In this study, we have characterized wild-type BPR and the color-tuning variant, Q105L, using a hybrid quantum mechanical/molecular mechanical (QM/MM) approach. We found that subtle differences in the interaction of Q105 with the PSB as well as variations in the HBN of the water cluster play a major role in regulating the  $(\lambda_{max})$  of BPR. The orientation of the Q105 side chain perturbs the bond length of C14-C15 in the PSB, while the orientation of internal water molecules in the binding pocket influences the strength of the HBNs, which, in turn perturbs the overall geometry of the PSB. Specifically, the bond length alternation (BLA) and torsion angle deviation (TAD) of the retinal polyene chain are shown to strongly depend on the strength of the HBNs in the BPR binding pocket.

### **■ COMPUTATIONAL METHODS**

System Construction. The initial structure was obtained from a snapshot of a  $\mu$ s-long molecular dynamics (MD) simulation based on the X-ray crystal structure of BPR in the dark state (PDB 4JQ6).<sup>20,22</sup> The snapshot was chosen as follows: all trajectory frames were screened for snapshots containing three water molecules in the region between the PSB, D97, and D227. An average structure of BPR (based on backbone heavy atoms) was then calculated, and the snapshot with the closest root-mean-square deviation (RMSD) to the average structure was selected for QM/MM calculations. Protonation states of titratable residues were consistent with the dark state of BPR: all acidic residues except E108 were deprotonated, and H75 was protonated on the  $N_{\delta}$  atom. The orientation of water molecules in the binding pocket was adjusted to (1) be consistent with the pentagonal water cluster typical of microbial rhodopsins that act as proton pumps and (2) study the effect of changes to the hydrogen-bonding network. Hydrogen atoms were added using PyMOL.<sup>23</sup> The initial structure was minimized with the molecular mechanics

(MM) method implemented in Gaussian09 using the AMBER force field (ff99sb),<sup>24,25</sup> in order to improve the HBNs mediated by internal water molecules in the binding pocket. The resulting orientation of water molecules (w1, w2, and w3) and the side chain of Q105 with respect to the retinyl chromophore are shown in Scheme 1. Nine variations of the retinyl chromophore binding pocket were studied in this work, in order to characterize the color tuning switch (Q105) and the water-mediated HBN (Scheme 1). Groups I, II, and III designate the three types of interactions of Q105 with the SB linkage. In Group I, the side chain oxygen atom (O<sub>e</sub>) in Q105 points toward Ha of C15 in retinal, whereas in Group II the  $N_e$ of Q105 is pointed toward H<sub>2</sub>. In Group III, Q105 is mutated to leucine (Q105L). The mutation was carried out in MacMolPlot, 26 with orientation of the side chain chosen to minimize potential steric interactions with neighboring water molecules in the cytoplasmic half-channel of the protein. There are three sub models for each group with distinct HBNs, (1, 2, and 3). In sub model 1, the two oxygen atoms, denoted O<sub>c</sub> and O<sub>d</sub>, of the D227 side chain participate in the HBN. In sub models 2 and 3, only one oxygen atom, Oc, in the D227 side chain participates in the HBN. The difference between sub models 2 and 3 is that they have different hydrogen atom orientations of two of the waters (w2, w3) that form the pentameric HBN (Scheme 1 and Figure S2).

QM/MM Calculations. The QM region includes the PSB plus the binding pocket residues D97, Q105, D227, and K231 and three water molecules (w1, w2, and w3) that are hydrogen-bonded to the SB, D97, and D227 (Figure 1 and Scheme 1). Geometry optimizations for the QM region were performed using the Gaussian09 package,<sup>24</sup> with the B3LYP/6-31G(d) basis set. The MM region was treated using the Amber force field (ff99sb).<sup>25</sup> The resulting QM/MM optimized structure was compared with the starting X-ray crystal structure, (PDB 4JQ6),<sup>20</sup> using the RMSD:

$$RMSD = \sqrt{\frac{\sum (r_{opt} - r_{c})^{2}}{n}}$$
 (1)

where  $r_{\text{opt}}$  and  $r_{\text{c}}$  are the intramolecular distances in the optimized and X-ray crystal structures, respectively. The red lines in Scheme 1 represent the distances used in eq 1. The retinyl chromophore in vacuo was optimized at the B3LYP/6-31G(d) level of theory to quantify the effect of strain/ deformation on color-tuning in BPR.

Table 1. Calculated Energies and Spectral Absorption Wavelengths of Retinal

			I				II		III			
model	crystal <sup>a</sup>	ret <sup>b</sup>	1	2	3	1	2	3	1	2	3	
rel E/eV <sup>c</sup>	_	-	6.14	0.00	1.79	5.50	0.14	1.99	5.32	0.00	1.25	
rel E ret <sup>d</sup>	_	0.00	0.34	0.40	0.35	0.29	0.40	0.35	0.26	0.46	0.34	
H-bond/eV	_	_	-6.67	-7.13	-6.92	-6.71	-7.18	-6.90	-6.62	-7.00	-6.92	
UV/nm <sup>e</sup>	490 <sup>f</sup>	_	501	496	499	493	505	500	509	534	515	

"X-ray structure (PDB 4]Q6). 16 bOptimized in gas phase at B3LYP/6-31G(d) using Gaussian09. Relative energies with respect to the most stable structure (submodel 2 for group I). Relative energies with respect to energy of retinal in the gas phase. Computed absorption wavelength ( $\lambda_{max}$ ) using the TD-DFT method. FExperimental value obtained from refs 1 and 2.

**Spectroscopic Calculations.** Optimized structures in the dark state were used to calculate the  $S_0 \rightarrow S_1$  vertical excitation energies. All atoms except the retinal chromophore were treated as point charges using results from our geometry optimization calculations. TD-DFT calculations were carried out as implemented in the Gaussian09 package at the B3LYP/ 6-31G(d) level of theory. 24,27

#### RESULTS AND DISCUSSION

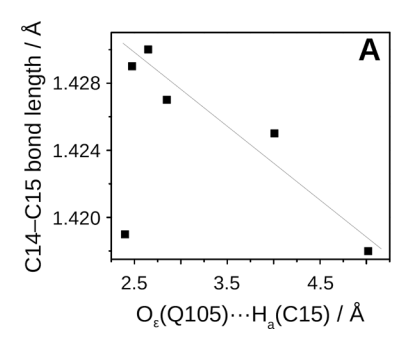
Optimized Structure of BPR in the Dark State. In order to understand the role of Q105 and the HBNs in the binding pocket, three main groups of retinal binding pocket configurations (I, II, and III) and three submodels for each configuration (1, 2, and 3) were considered (see Methods). With an overall RMSD of <1.15 Å, each conformation is in good agreement with the X-ray structure. In Group I (I.1, I.2, and I.3), the  $O_{\epsilon}(Q105)$ ...C15 distances, 3.394, 3.628, and 3.485 Å, respectively, are shorter than those found in the X-ray structure (4.056 Å),<sup>20</sup> while they are significantly longer in Group II (5.927, 3.864, and 4.986 for II.1, II.2, and II.3) (Figure 2 and Table S2). The C-O bond lengths of the aspartic acids that participate in the HBN with D97 and D227 are longer compared to the nonparticipating (C-O<sub>d</sub>) bond length of D227 (Figure 2 and Table S2). The C-O bond length was subsequently lengthened by about 0.02 Å through a hydrogen-bonding interaction. In each group, submodel 2 is more stable than submodels 1 and 3 by about 6 and 2 eV, respectively, as shown in Table 1. Despite the greater overall stability of submodel 2, submodel 1 has a slightly more stable PSB (~0.1 eV), indicating that both Q105 and the hydrogenbonding network make important contributions to the electronic environment of the retinal binding pocket.

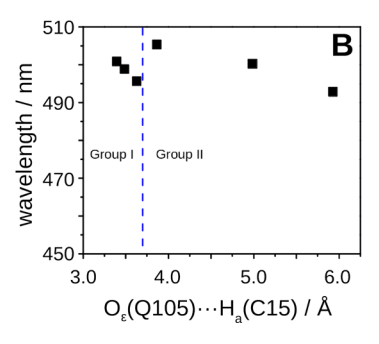
The optimized structural models were validated by calculating the  $\lambda_{max}$  of the following systems: (1) a QM optimized PSB geometry in vacuo, (2) an X-ray crystal structure of retinal in solution (CSD-JIHFAH),<sup>28</sup> and (3) the QM/MM optimized PSB geometry in the protein environment using TD-DFT (Gaussian) approaches. Upon confirming that the geometry of the retinal binding pocket was consistent with the X-ray crystal structure of BPR, we determined the spectral absorption characteristics for each group and submodel. The values of calculated spectroscopic wavelengths by TD-DFT for the BPR variants of group I were 501, 496, and 499 nm for submodels 1, 2, and 3, respectively (Table 1). Likewise, the calculated wavelengths for group II were 493, 505, and 500 nm for submodels 1, 2, and 3 (Table 1), in good agreement with the  $\lambda_{\rm max}$  of BPR (~490 nm). The  $\lambda_{\rm max}$  of the Q105L variants (Group III) were red-shifted to 508, 534, and 515 nm for submodels 1, 2, and 3, also in good agreement with the experimental  $\lambda_{max}$  of the corresponding BPR point mutant (515 nm). The I.2 conformation is the most stable (all other

energies are calculated relative to this conformation, Table 1) and also within 5 nm of the experimental  $\lambda_{max}$ . Submodel 1 is energetically unstable by more than 5 eV compared to the other submodels (2 and 3). The reason for this discrepancy is unclear because the other two energy contributions (H-Bond energy of the binding pocket and the relative energy of retinal) are similar among all submodels. The most likely explanation is that submodel 1 has slightly larger intermolecular distances between the PSB and the water cluster (see the Results and Discussion section below).

Our calculations show that if the orientation of Q105 has an effect on the  $\lambda_{max}$  of BPR, they are very subtle. In each of the three submodels in groups I and II, the side chain of Q105 is between 4 and 5 Å from the PSB: in all cases, rotation of the carbonyl group is closest to the PSB (Figure S3). In addition, one or two water molecules coordinate with the side chain of Q105 to help stabilize its orientation. For submodels 1 and 3, this coordination leads to an orthogonal orientation of the terminal group, whereas in submodel 2 the carbonyl and amide groups are parallel to the plane of the polyene chain (Figure S2). A recent spectroscopic study on GPR determined that the color-tuning switch is affected by a combination of spatial restraints (i.e., volume of the amino acid side chain) and electronic interactions at position 105, where larger amino acid side chains were hypothesized to partially disrupt the hydrogen-bonded network involving the PSB, leading to a red-shift in spectral wavelengths.<sup>30</sup> This makes sense in comparison to our results, as the only difference among submodels in groups I and II is the orientation of Q105 and corresponding coordination with water molecules, with differences in  $\lambda_{max}$  of 8, 9, and 1 nm, respectively. Weaker electrostatic interactions in the retinal binding pocket can induce red-shifted  $\lambda_{max}$ , as reported previously when Q105 was mutated to leucine. The  $\lambda_{\rm max}$  is influenced by the conformation of the amide group of Q105 and the bond length of C14-C15. However, it is not clear if the bond length is modulated solely by the attractive interaction between O105 and H<sub>a</sub>(C15), as the bond length of C14-C15 has a strong linear dependence on the strength of the HBN in the binding pocket. Details of the color-tuning mechanism of BPR are described below.

Role of Q105 in Conformation of Retinal Binding **Pocket.** In group I, the  $O_{\epsilon}$  atom of Q105 forms a weak interaction by pointing toward the C15 hydrogen of retinal. The  $O_{\epsilon}(Q105)\cdots H_{a}(C15)$  distances of 2.397, 2.646, and 2.473 Å for models I.1, I.2, and I.3, respectively, are much longer than a typical hydrogen bond (1.6–2.0 Å) (Figure 2 and Table S2). These weak interactions slightly alter the geometry of retinal compared to groups II and III. Most notably, the C14-C15 bond for group I (1.419, 1.430, and 1.429 Å) are extended by about 0.003 Å (Table S3). An inverse relationship emerges





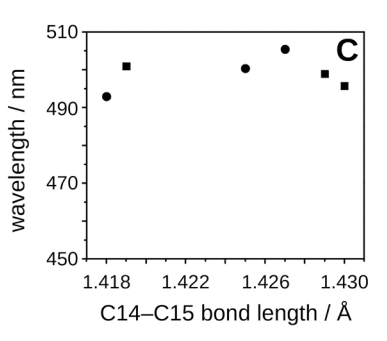


Figure 3. Interactions of Q105 with retinal directly affect bond character of the polyene chain but are weakly coupled to  $\lambda_{max}$  in the dark state. (A) Bond length of C14–C15 in retinal as a function of distance between  $O_{\epsilon}(Q105)$  and  $H_a(C15)$  of retinal. (B) Computed  $\lambda_{max}$  as a function of distance between  $O_{\epsilon}(Q105)$  and  $H_a(C15)$ . Dashed line separates calculations of group I configurations (left) from group II configurations (right). (C) Computed  $\lambda_{max}$  as a function of bond length of C14–C15 in retinal.  $\blacksquare$ : group I configurations;  $\blacksquare$ : group II configurations.

Table 2. Calculated Intermolecular Distances between the PSB and the Water Cluster in BPR

		I			II			III	
model	1	2	3	1	2	3	1	2	3
$H_b \cdots O_{w1}$	1.55	1.45	1.49	1.58	1.45	1.48	1.57	1.47	1.58
$H2\cdots O_b$	1.72	1.67	1.67	1.71	1.70	1.68	1.73	1.69	1.66
H1···O <sub>c</sub>	1.76	1.62	1.70	1.79	1.65	1.70	1.79	1.63	1.70
$N_{SB} \cdots O_{w1}$	2.61	2.55	2.58	2.63	2.55	2.57	2.63	2.57	2.57

between the bond length of C14-C15 and the  $O_{\epsilon}(Q105)\cdots$  $H_a(C15)$  distance: as the  $O_e$  of Q105 attracts  $H_a(C15)$ , the C14-C15 bond length increases (i.e., weakens the bond) (Figure 3a). The lengthening of the C14-C15 bond is accompanied by a decrease in the bond lengths of C13=C14 and C15=NSB, indicating that Q105 acts to withdraw electrons from the vicinity of C15 in the polyene chain through the weak attractive interaction between  $O_{\epsilon}(Q105)\cdots$ H<sub>2</sub>(C15). This deshielding effectively weakens the conjugation of the polyene chain in the vicinity of C15. Our results agree with recent solid-state NMR work in which the C14-C15 bond was considerably lengthened (~0.04 Å) by interactions with Q105, leading to an extension of the "conjugation defect" localized around the SB linkage. The attractive interaction also perturbs the C13=C14-C15=NSB dihedral angle which in turn affects the planarity and/or conjugation of the retinal polyene chain.

In the solid-state NMR study carried out by Glaubitz and coworkers, they saw a two-degree shift in the H–C14–C15–H dihedral between GPR and the L105Q blue-shifted variant. They hypothesized that the color-tuning mechanism from the L105Q mutation was due to enhanced interactions between Q105 and the  $H_a$ –C15 bond, leading to an increase in the bond length of C14–C15. However, in our calculations the  $H_a$ –C15 and C14–C15 bonds are not directly influenced by interactions with Q105; the bond lengths of 1.087 and 1.419 Å in model I.1, respectively, are nearly identical to those in model II.1 and III.1 (Table S2). In addition, the  $H_b$ –N $^+$ (SB) and  $H_{b(SB)}$ ····O(w1) bonds do not show any relation to changes in interaction with Q105 (Table 2).

The discrepancies between our QM/MM results and those of Glaubitz and co-workers highlights the fact that the environment surrounding residue 105 must also be accounted for with respect to the color-tuning mechanism of PR. Birge and co-workers carried out semiempirical calculations on homology models of both GPR and BPR (this was conducted before solution of the structures for each protein). 31,32 It was determined that the carbonyl group of the Q105 side chain

altered the electrostatic environment around C14, C15, and the SB, ultimately leading to the blue-shift in the  $\lambda_{\rm max}$  that is characteristic of BPR. Most importantly, they determined that this blue shift was solely dependent on orientation of the side chain of Q105 toward the SB, regardless of formation of a hydrogen bond between Q105 and the  $H_a(C15)$ . In addition, a comparison between the NMR structure of GPR and the X-ray crystal structure of BPR reveals numerous differences between the retinal binding pockets, from the orientation of the Schiff base conjugation from the side of K231 to the arrangement of aromatic side chains along the polyene chain and the  $\beta$ -ionone ring. O1,33 This further underscores how the retinal binding pockets for each variant of PR are not equivalent to each other.

The interaction of Q105 has a very subtle influence on the  $\lambda_{\rm max}$  of BPR in the dark state. Regardless of the participating atom of Q105 in the interaction ( $O_{\epsilon}$  or  $N_{\delta}$ ) with the  $H_{\rm a}({\rm C15})$  of retinal, there is an inverse relationship between the distance of  $O_{\epsilon}({\rm Q105})\cdots H_{\rm a}({\rm C15})$  and the  $\lambda_{\rm max}$  (Figure 3b). This relationship is much more sensitive to changes in that distance when the  $O_{\epsilon}$  of Q105 is participating in the interaction (i.e., group I). The same relationship does not hold true for the C14–C15 bond length and  $\lambda_{\rm max}$ : in group I it is inverse, whereas in group II it is a direct relationship (Figure 3c). Although this does not fully account for the modulation of  $\lambda_{\rm max}$  in BPR, these specific interactions show how Q105 can influence the spectral properties of PR without greatly perturbing the retinal chromophore.

Contribution of the Hydrogen Bond Network to Color Tuning. Submodels 1, 2, and 3 possess different hydrogen-bonded networks within the binding pocket due to distinct orientations of water molecules w2 and w3. These water-mediated networks have been characterized theoretically for other retinal proteins such as bR, and it is known that water orientation strongly affects hydrogen-bonding strength in the binding pocket. Hydrogen bond energy was calculated for retinal, D97, D227, and the 3 water molecules (w1, w2, and w3) using the following equation:

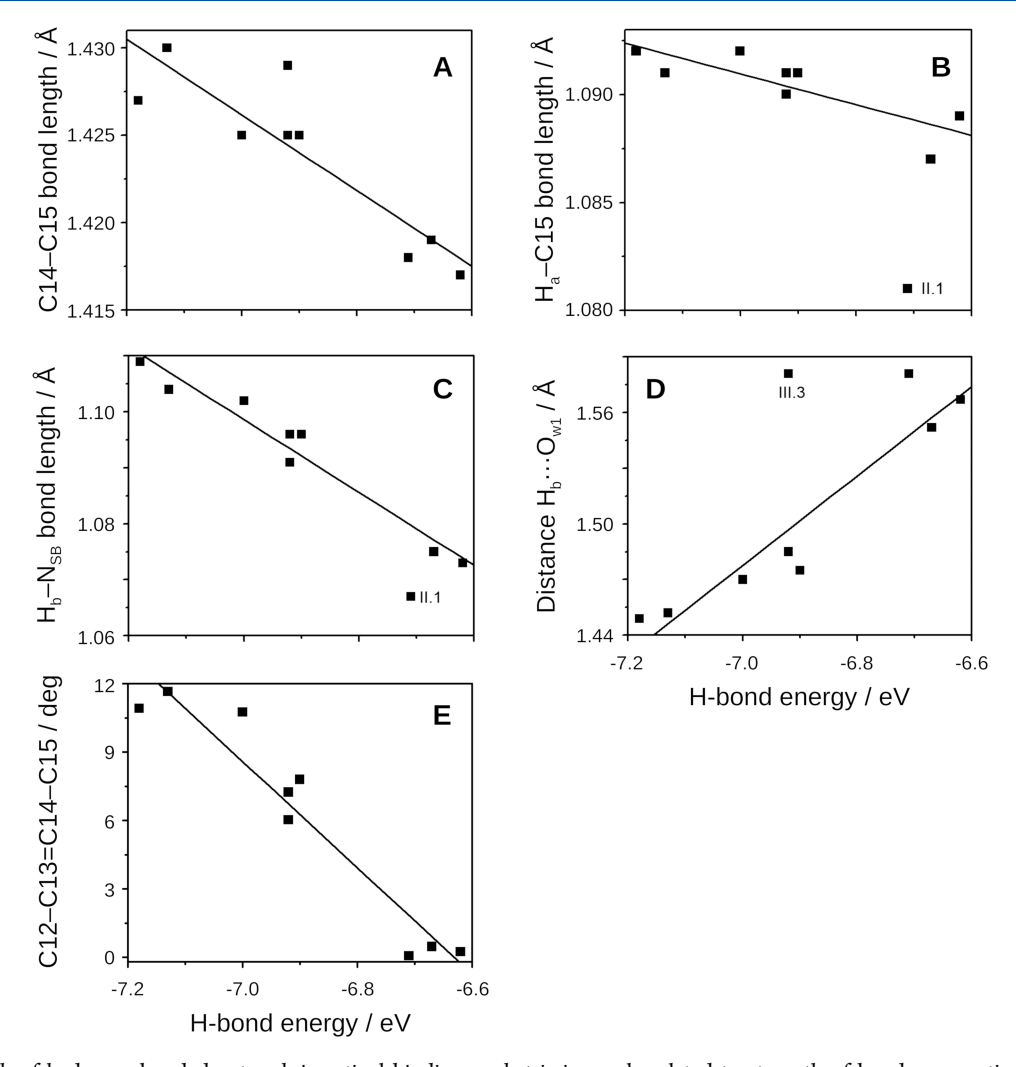


Figure 4. Strength of hydrogen-bonded network in retinal binding pocket is inversely related to strength of bonds near retinal Schiff base. (A) Hydrogen bond energy as a function of C14–C15 bond length in retinal. (B) Hydrogen bond energy as a function of C15– $H_a$  bond length in retinal. (C) Hydrogen bond energy as a function of H<sub>b</sub>–N<sub>SB</sub> bond length in retinal. (D) Hydrogen bond energy as a function of hydrogen bond distance between H<sub>b</sub> in retinal and O of w1. (E) C12–C13=C14–C15 dihedral angle of retinal as a function of hydrogen bond energy. Twist of retinal polyene chain from planar configuration strengthens hydrogen-bonded network within retinal binding pocket.

$$E_{\text{hbond}} = E_{\text{water}} + E_{\text{HCO}_2} + E_{\text{ret}} + E_{\text{total}}$$
 (2)

where  $E_{\rm HCO_2^-}$  and  $E_{\rm water}$  are the energies of the optimized structure of each molecular component in the gas phase and  $E_{\rm ret}$  and  $E_{\rm total}$  are the single point energies of the retinal chromophore and the residues extracted from the optimized BPR structure, respectively. ( $E_{\rm ret}$  accounts for the K231 side chain by treating it as an ethyl group.) Submodel 2 has the most stable HBN. The hydrogen bond energy follows the same trend as the calculated total energy of the system, increasing in the following order: submodel 2 < 3 < 1. The calculated hydrogen bond energy differences between submodels 1 and 2 are about 0.4 eV, whereas those between submodels 2 and 3 are about 0.2 eV (Table 1).

Careful examination of the counterion complex reveals subtle differences in each HBN. For submodel **2**, the two counterion residues, D97 and D227, have an average length of 1.26 Å for the C–O bond of the carboxylate group (Figure 2 and Table S2). However, participation in the HBN leads to elongation of the bond (1.29 Å in D227 and 1.27 Å in D97). In submodel **1**, the bond length difference between C–O<sub>c</sub> and C–O<sub>d</sub> of D227 is about 0.03 Å, while it is about 0.06 Å in

submodels 2 and 3. The hydrogen bond length between  $O_c(D227)\cdots H_1(w1)$  is almost 1.8 Å in submodel 1, while it is 1.7 Å or shorter in submodels 2 and 3 (Table 2). Another hydrogen bond, O<sub>d</sub>(D227)···H<sub>5</sub>(w3) in submodel 1, is longer than 1.9 Å, whereas the corresponding hydrogen bond in submodels 2 and 3  $(O_c(D227)\cdots H_s(w3))$  is shorter than 1.9 Å. Overall, the hydrogen bonds formed by D227 are longer in submodel 1 compared to submodels 2 and 3. Although it is unclear how these differences originated, the polar residues Y76 and R94 could play a direct role in this effect. R94 forms a hydrogen bond to w2 in submodels 2 and 3 but shifts to form a hydrogen bond to w3 in submodel 1. The shift of the R94 side chain to interact with w3 destabilizes the hydrogen-bonded interaction between D227 and w3. We also recently showed that R94 plays a potentially important role facilitating hydration between the retinal binding pocket and the extracellular region of PR where proton release to the periplasm takes place.<sup>22</sup> In addition, the polar residue Y76 takes part in the difference between submodel 2 and 3. H<sub>4</sub> of w2 forms a hydrogen bond to Y76 in submodels 1 and 2, but H<sub>6</sub> of w3 does not point to Y76 in submodel 3 (Figure S2). In general, the shift in the different orientation of the water

Table 3. Measured and Calculated Dihedral Angles of Retinal

				I			II			III		
model	crystal <sup>a</sup>	ret <sup>b</sup>	$\operatorname{ret}^c$	1	2	3	1	2	3	1	2	3
C12-C13=C14-C15	-179.7	-179.8	-175.5	179.5	-168.4	-172.8	-179.9	-169.1	-172.2	179.8	-169.3	-174.0
$C13 = C14 - C15 - H_a$	_	-0.1	_	16.0	-0.8	6.4	-4.7	-1.5	4.6	3.9	-1.7	6.1
$C14-C15=N_{SB}-C$	-179.5	179.6	-174.4	-165.3	176.1	-175.6	174.6	175.6	-177.5	-176.9	175.3	-175.6
$C-C15=N_{SB}-H_b$	-	0.7	_	-8.7	-0.6	-0.2	-0.9	-0.8	-0.5	-3.3	-1.6	-1.1

<sup>&</sup>lt;sup>a</sup>X-ray structure from PDB 4JQ6. <sup>20</sup> <sup>b</sup>Optimized in gas phase at B3LYP/6-31G(d) using Gaussian09. <sup>c</sup>X-ray structure of *N*-Methyl-*N*-phenylretinal iminium perchlorate (Ref code: JIHFAH) from the CSD. Note that the SB nitrogen atom is attached to an aromatic ring, and a perchlorate ion is present near the β-ionone ring.

molecules in the binding pocket induces different hydrogen bond formation to the polar amino acid residues, modulating the strength of the hydrogen-bonded network in PR.

Although the calculated  $\lambda_{max}$  does not show a linear dependency on hydrogen bond strength, a red shift occurs with increasing hydrogen bond strength in groups II and III and a blue shift occurs in group I (Table 1). The most noticeable influence of hydrogen bond strength is with respect to the structural arrangement of the retinal binding pocket. A strong relationship exists between the hydrogen bond energy and selected bond lengths in the binding pocket, C14-C15,  $H_a$ -C15,  $H_b$ -N<sup>+</sup><sub>SB</sub>, and  $H_b$ ···O(w1) (Figure 4a,b and Table 3). Three of the bonds (C14-C15,  $H_a$ -C15, and  $H_b$ - $N_{SB}^+$ ) stretch with increasing hydrogen bond strength. The C14-C15 bond is codependent on hydrogen bond strength and the interaction of  $O_{\epsilon}(Q105)\cdots H_{a}(C15)$ , displaying a more linear dependency on the former than the latter. In particular, the bond length of H<sub>b</sub>-N<sup>+</sup><sub>SB</sub> and the hydrogen bond interaction of H<sub>b,SB</sub>···O(w1) are strongly and directly influenced by the hydrogen bond energy (Figure 4c,d). The double bonds closest to the Schiff base linkage, C13=C14 and C15=N<sub>SB</sub>, have bond lengths largely unchanged with fluctuations in hydrogen bond strength, but the C12-C13=C14-C15 dihedral undergoes an increase in twist from planarity with a corresponding increase in hydrogen bond strength (Figure 4e). Although hydrogen bond strength is not directly correlated with  $\lambda_{\text{max}}$ , it influences the electronic structure of the polyene chain in the retinal chromophore by withdrawing electrons from the hydrogen of the Schiff base. In general, the arrangement of hydrogen bonds are also a strong indicator of structural changes within the retinal binding pocket, especially close to the Schiff base.

Comparison to Retinal Ligands and Other Retinal **Proteins.** It is useful to supplement theoretical conformational predictions with experimentally observed conformational preferences in the crystalline state, where crystal packing forces may exert a strong effect on molecular conformations. We compared the QM/MM optimized PSB geometry in BPR with the conformational preferences of the N-methyl-N-phenyl retinal iminium perchlorate compound taken from the Cambridge Structural Database (CSD refcode: JIHFAH). Comparison of the bond lengths and dihedral angles reveal that (a) crystal packing effects and (b) competition between intra- and intermolecular forces (e.g., in a protein binding site) play a role in enforcing a strained conformation on retinal, which in turn leads to the red shift of the chromophore in BPR. With respect to bond lengths, the C11=C12 and C13= C14 double bonds are most similar between the crystallized retinal ligand and the optimized structure within the protein (Table S2). However, the retinal binding pocket contributes to a lengthening of the single bonds near the Schiff base (C12-

C13 and C14–C15) as well as in the double bonds near the  $\beta$ ionone ring. The longer single bonds near the Schiff base (about 0.02-0.03 Å) are most likely due to the enhancement of charge separation from the electrostatic interactions between the Schiff base and the counterion and complex counterion of BPR, D97, and D227. The longer double bonds near the  $\beta$ -ionone ring (C5=C6 and C7=C8) could be due to the additional twist imposed by the retinal binding pocket on the corresponding dihedral angles (C5=C6-C7=C8 and C7=C8-C9=C10, Table S3). The orientation of the pentagonal water cluster also influences the twist of the retinal polyene chain with respect to the crystallized retinal ligand. For the JIHFAH structure, the series of dihedrals from C10-C11=C12-C13 to C13=C14-C15=N alternates into (>180°) and out of (<180°) the plane, and submodel 2 mirrors this behavior (Table S3). In contrast, submodel 1 has the opposite orientation of the polyene chain, and submodel 3 displays a gradual increase into the plane in the twist of the polyene chain.

The  $\lambda_{max}$  of retinal proteins strongly depend on the structure of the polyene chain in the chromophore and its interaction with the surrounding protein environment. $^{34,40-42}$  In the case of PR, the geometry of the retinal binding pocket has been optimized to absorb available light in specific wavelength ranges. The polyene chain bond length of retinal between C9 and C15 is more alternated and the plane of the polyene chain is more twisted compared to retinal in the gas phase (Figure 5a,b and Table S3). In particular, aromatic amino acid residues play a critical role in stabilizing unfavorable conformations of the retinal polyene chain. For example, the side chain of Y200 in GPR (Y201 in BPR) sterically hinders the isomerization of the C13=C14 double bond involved in photoactivation through direct interactions with C14 of retinal.<sup>43</sup> Our earlier discussion highlighted how the residue at position 105 also plays a role in the dark  $\rightarrow$  K  $\rightarrow$  M transition in GPR. In the case of bacteriorhodopsin, the homologous tyrosine residue (Y185) plays a critical role in modulating the electrostatic environment around the PSB, leading to efficient photoisomerization and proton transfer.44

The  $\lambda_{max}$  of retinal proteins can also be expressed as a function of the bond length alternation (BLA):  $^{34,40,42}$ 

$$BLA = \frac{\sum_{i}^{n_i} r_{i,\text{single bond}}}{n_i} - \frac{\sum_{j}^{n_j} r_{j,\text{double bond}}}{n_j}$$
(3)

The first and second terms on the right-hand side are average bond lengths of single and double bonds, respectively. The bond length alternation is influenced by the strength of the hydrogen-bonded network (Figure 6a), due to its direct interaction with the C14–C15 and C15—NSB bonds (i.e., a corresponding increase). In addition, the BLA is inversely

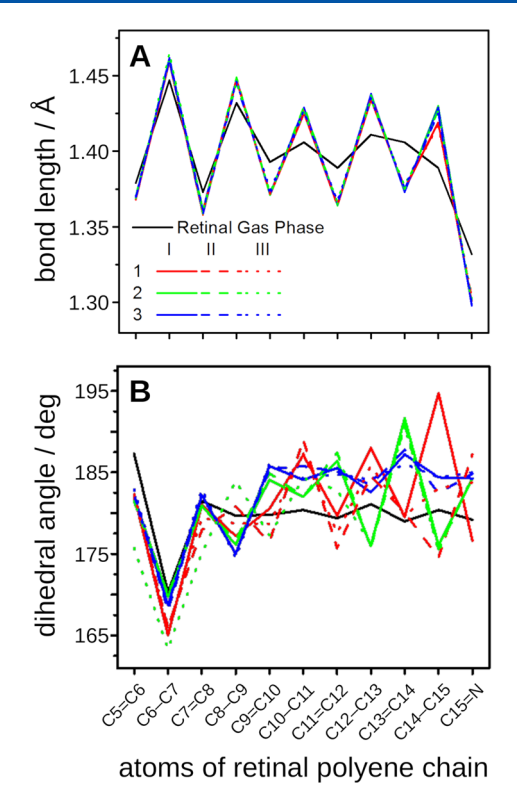


Figure 5. Bond length in retinal is largely unaffected by twist of the polyene chain. (A) Bond length along retinal polyene chain. Black: Gas-phase calculation of retinal; red line: group I.1; red dashed: II.1; red dots: III.1; green line: group I.2; green dashed: II.2; green dots: III.2; blue line: group I.3; blue dashed: II.3; and blue dots: III.3. (B) Torsional angle deviation along retinal polyene chain. Color scheme is identical to part A.

proportional to the interatomic distance of  $O_{\epsilon}(Q105)\cdots$   $H_a(C15)$  (except for I.1) (Figure 6b). The BLAs are also smaller in the Q105L mutated system compared to that in Group I. In our study,  $\lambda_{\rm max}$  does not show a strong correlation with the BLA, generally decreasing as the BLA increases. However, if the models are organized according to the planarity of their C12–C13=C14–C15 dihedral angles ("flat" models:  $|\phi_{C12-C13=C14-C15}-180| < 5^{\circ}$  and "twist" models:  $|\phi_{C12-C13=C14-C15}-180| > 5^{\circ}$ ),  $\lambda_{\rm max}$  shows a linear relationship with the BLA, as shown in Figure 6c.

The  $\lambda_{max}$  of retinal proteins is also influenced by the planarity of the retinal polyene chain; deviation from planarity alters the conjugation system of  $\pi$ -orbitals.<sup>45</sup> This twist in the polyene chain destabilizes the ground state,  $S_0$ , allowing for progression through the  $S_1$  excited state and producing the first photointermediate, the K state.<sup>46</sup> The torsional angle deviation (TAD) shows the deviation from planarity of the retinal polyene chain:

$$TAD = \frac{\sum_{i}^{N} (180^{\circ} - |\phi_{i}|)}{N}$$
(4)

where N is the total number of torsional angles and  $\phi_i$  is the ith torsional angle between C5 and  $N_{SB}$ . The torsional angle deviation has a linear relationship with the computed  $\lambda_{max}$  except at III.1, as shown in Figure 7. Essentially, wavelength undergoes a red shift with increasing TAD values. Based on these results, the TAD roughly depends on two parameters, the hydrogen bond energy and the relative energy of the retinal

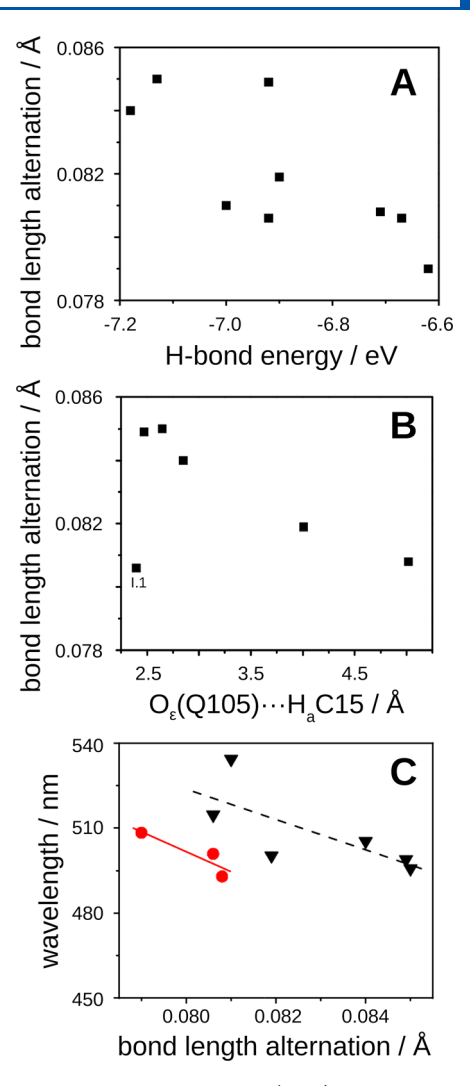


**Figure 6.** Bond length alternation (BLA) is directly related to hydrogen-bonded energy and  $\lambda_{\rm max}$  in BPR. (A) BLA as a function of hydrogen bond energy. (B) BLA as a function of distance between the O<sub>ε</sub> of Q105 and H<sub>a</sub>(C15). (C) Computed wavelength as a function of bond length alternation. Dashed lines are a linear fit, with a  $R^2$  value of about 0.9 for the twist model ( $\blacktriangledown$ ) and 0.7 for the flat model (red  $\blacksquare$ ). Flat:  $|\phi_{C12-C13=C14-C15}-180| > 5^\circ$ .

chromophore (i.e., the energy difference between the retinal structure from the protein and that from the retinal chromophore in the gas phase). TAD roughly increases with hydrogen bond strength but decreases with increasing relative energy of the retinal chromophore. Considering the overall relationship in Figure 7A,B, the TAD value shows roughly linear dependency on the relative energy ( $R^2 \approx 0.6$ ), but it does not on hydrogen bond strength ( $R^2 \approx 0.2$ ). The TAD value does not show a relationship with the BLA value (Figure S4). Both parameters, TAD and BLA, strongly depend on the interaction of retinal with the surrounding protein; they are very small in the gas phase (2–4 times smaller than in PR, Tables S2 and S3).

Another critical component in modulating the spectral absorption of retinal proteins is water molecules, which help regulate the HBN within the retinal binding pocket and the BLA of the retinal polyene chain. 42,47 Although our calculations provide a detailed description of this relationship in PR, comparisons with other microbial rhodopsins are much

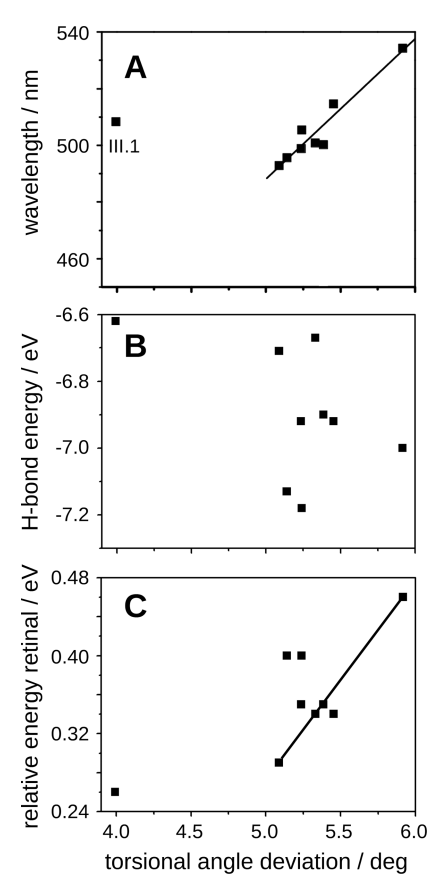


**Figure 7.** Twist of the retinal polyene chain in BPR leads to red shift in the calculated  $\lambda_{\text{max}}$ . (A) Computed wavelength as a function of torsional angle deviation value (TAD). Ignoring the outlier at **III.1**, the  $R^2$  value is 0.91. (B) Hydrogen bond energy as a function of TAD. (C) Relative retinal energy as a function of TAD.

more complex. With the rapid increase in availability of structural data of microbial retinal proteins, we can at least compare their respective BLAs of retinal with the BLA of the most stable optimized structure of BPR (I.2, Figure 8). High-

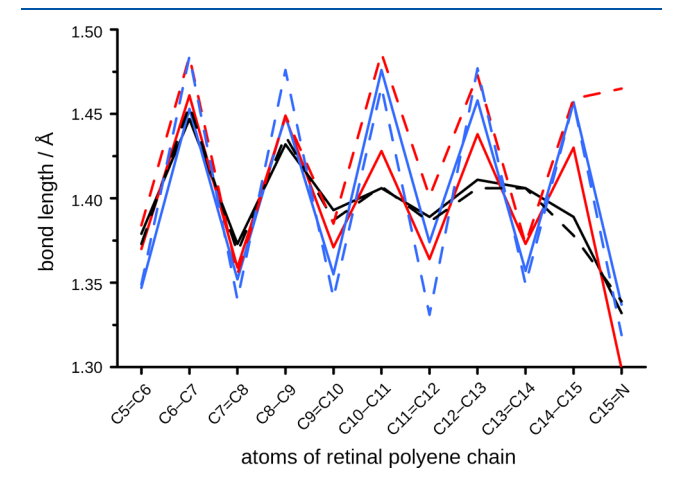


**Figure 8.** Polyene chain of retinal in PR has similar bond character to other retinal proteins. Bond length alternation values along retinal polyene chain. Black line: retinal in gas phase; red line: bPR model **I.2**; blue line: bacteriorhodopsin; black dashed line: halorhodopsin; red dashed line: xanthorhodopsin; and blue dashed line: *E. sibiricum* rhodopsin.

resolution crystal structures show us that bacteriorhodopsin (bR)<sup>48</sup> and halorhodopsin<sup>49</sup> possess similar HBNs in the binding pocket, involving three water molecules, a counterion residue, and the SB; xanthorhodopsin<sup>50</sup> and *E. sibiricum* rhodopsin<sup>51</sup> were chosen because they are evolutionally similar to BPR. Halorhodopsin is unique from the other retinal proteins in that it possesses a diamond-shaped water cluster instead of a pentagonal one.<sup>42</sup> In the pentagonal-shaped systems, H<sub>b,SB</sub> is directly hydrogen-bonded to w1, but in the diamond-shaped network, it is bonded to the Cl<sup>-</sup> ion.<sup>36,38,42,52</sup> BPR, bR, xanthorhodopsin, and *E. sibiricum* rhodopsin show similar bond length patterns, but halorhodopsin is quite different, especially between C9 and N<sub>SB</sub>, similar to retinal in the gas phase (Figure 8).

An examination of BLA and TAD values for a series of microbial retinal proteins shows that  $\lambda_{max}$  can be influenced by BLA and TAD, but that there are no discernible trends among these variables (Table S4). In some instances, it is possible to predict relative wavelengths between retinal proteins.<sup>53</sup> For example, the wavelength of halorhodopsin (578 nm) is redshifted by about 90 nm compared with that of BPR. The BLA and TAD values of halorhodopsin are 0.040 Å (smaller than BPR) and 7.4° (larger than BPR), respectively. In bR ( $\lambda_{max}$  = 568 nm), the relationship is more ambiguous: the BLA of 0.105 Å is larger than and the TAD of 5.0° is similar to BPR, indicating that the former (BLA) may contribute to a red-shift in  $\lambda_{max}$ . bR has a very similar HBN to BPR, so it is assumed that  $\lambda_{max}$  is more influenced by interactions with the surrounding protein than the hydrogen bond strength when comparing the two systems.

We must caution that a multitude of factors besides BLA and TAD contribute to the photoexcitation process. S4,55 It is common for perturbations to the retinal distal from the Schiff base linkage to influence the spectral absorbance of retinal proteins. In the case of channelrhodopsin, an introduction of a double mutant forced a twist of the C5=C6-C7=C8 dihedral angle from 174.4° to -27.7°, leading to a blue-shift in  $\lambda_{\rm max}$  from 476 to 455 nm. S6 Archaerhodopsin-3 also showed a drastically blue-shifted  $\lambda_{\rm max}$  as a result of large-scale changes in the C5=C6-C7=C8 dihedral. In contrast, introduction of modifications to the  $\beta$ -ionone ring of retinal in PR can lead to red-shifts of  $\lambda_{\rm max}$  to the near-infrared region of the electromagnetic spectrum.

Although retinal proteins universally cause a red-shift in the spectral characteristics of the retinal chromophore, very subtle differences in the local environment of the binding pocket lead to a wide distribution in the magnitude of this red-shift. This holds true both for similar proteins such as GPR and BPR as well as other microbial retinal proteins. The structural arrangement of retinal strongly depends on the HBN and spatial orientation of surrounding amino acid residues. Two structural parameters, BLA and TAD, are valuable indicators of this relationship between hydrogen bonding and protein-chromophore interactions, leading to a fuller understanding of their effect on  $\lambda_{\rm max}$  in retinal proteins.

**Conclusions.** A fundamental understanding of the colortuning mechanism in BPR is obtained by investigating nine different structural models of the dark-adapted BPR binding pocket using hybrid QM/MM methods. The QM/MM geometries are in good agreement with the X-ray structure of BPR, and the computed  $\lambda_{\rm max}$  using the TD-DFT and SORCI +Q methods are also in good agreement with experimental observations. We find that the strength of the hydrogen-

bonded network in BPR is strongly influenced by the orientation of water molecules in the binding pocket. The most stable pentagonal cluster (submodel 2) fully utilizes the water molecule bound to the complex counterion, D227. Although direct interactions of Q105 with the retinal chromophore leads to stretching of the C14–C15 bond, the  $\lambda_{\rm max}$  of BPR is more dependent on the BLA and TAD of the entire polyene chain. The  $\lambda_{\rm max}$  is blue-shifted with increasing BLA but red-shifted with increasing TAD. Both are influenced by two parameters, the hydrogen bond strength and the relative energy of the retinal chromophore.

#### ASSOCIATED CONTENT

# **S** Supporting Information

The Supporting Information is available free of charge at https://pubs.acs.org/doi/10.1021/acs.jpcb.9b08189.

Figure S1, a multiple sequence alignment of microbial and animal rhodopsins highlighting the lack of conservation of a color-tuning switch similar to Q105 in BPR; Figure S2, a three-dimensional comparison of the pentagonal water clusters in submodels 1, 2, and 3 to highlight the differences in orientation of water molecules with respect to D97, D227, Y76, and R94 proximal to the retinal binding pocket; Figure S3, a three-dimensional comparison of the orientation of Q105 with respect to the PSB for submodels 1, 2, and 3; Figure S4, plot of the relationship between BLA and TAD; Tables S1-S3, list of key distances and dihedral angles in the retinal binding pocket; and Table S4, comparison of spectral absorption wavelengths with bond length alternation and torsional angle deviation between blue proteorhodopsin and other retinal proteins (PDF)

#### AUTHOR INFORMATION

## **Corresponding Author**

\*E-mail: blake.mertz@mail.wvu.edu.

ORCID

Blake Mertz: 0000-0002-7677-0496

**Notes** 

The authors declare no competing financial interest.

# ■ ACKNOWLEDGMENTS

The authors thank the Cambridge Crystallographic Data Centre for access to the JIHFAH crystal structure. This work was supported by West Virginia University (B.M.), the WVU NanoSAFE program NSF EPS-1003907 (C.L.), and NSF MCB-1714888 (B.M.). Computational time was provided through WVU Research Computing.

# REFERENCES

- (1) Béjà, O.; Aravind, L.; Koonin, E. V.; Suzuki, M. T.; Hadd, A.; Nguyen, L. P.; Jovanovich, S. B.; Gates, C. M.; Feldman, R. A.; Spudich, J. L.; et al. Bacterial Rhodopsin: Evidence for a New Type of Phototrophy in the Sea. *Science* **2000**, *289*, 1902–1906.
- (2) Béjà, Ó.; Spudich, E. N.; Spudich, J. L.; Leclerc, M.; DeLong, E. F. Proteorhodopsin Phototrophy in the Ocean. *Nature* **2001**, *411*, 786–789
- (3) Marchetti, A.; Catlett, D.; Hopkinson, B. M.; Ellis, K.; Cassar, N. Marine Diatom Proteorhodopsins and Their Potential Role in Coping with Low Iron Availability. *ISME J.* **2015**, *9*, 2745–2748.

- (4) Walter, J. M.; Greenfield, D.; Bustamante, C.; Liphardt, J. Light-Powering Escherichia Coli with Proteorhodopsin. *Proc. Natl. Acad. Sci. U. S. A.* **2007**, *104*, 2408–2412.
- (5) Ernst, O. P.; Lodowski, D. T.; Elstner, M.; Hegemann, P.; Brown, L. S.; Kandori, H. Microbial and Animal Rhodopsins: Structures, Functions, and Molecular Mechanisms. *Chem. Rev.* **2014**, *114*, 126–163.
- (6) Dioumaev, A. K.; Brown, L. S.; Shih, J.; Spudich, E. N.; Spudich, J. L.; Lanyi, J. K. Proton Transfers in the Photochemical Reaction Cycle of Proteorhodopsin. *Biochemistry* **2002**, *41*, 5348–5358.
- (7) Man, D.; Wang, W.; Sabehi, G.; Aravind, L.; Post, A. F.; Massana, R.; Spudich, E. N.; Spudich, J. L.; Beja, O. Diversification and Spectral Tuning in Marine Proteorhodopsins. *EMBO J.* **2003**, 22, 1725–1731.
- (8) Amsden, J. J.; Kralj, J. M.; Bergo, V. B.; Spudich, E. N.; Spudich, J. L.; Rothschild, K. J. Different Structural Changes Occur in Blueand Green-Proteorhodopsins during the Primary Photoreaction. *Biochemistry* **2008**, *47*, 11490–11498.
- (9) Mao, J.; Do, N.-N.; Scholz, F.; Reggie, L.; Mehler, M.; Lakatos, A.; Ong, Y.-S.; Ullrich, S. J.; Brown, L. J.; Brown, R. C. D.; et al. Structural Basis of the Green-Blue Color Switching in Proteorhodopsin as Determined by NMR Spectroscopy. *J. Am. Chem. Soc.* **2014**, *136*, 17578–17590.
- (10) Lakatos, M.; Lanyi, J. K.; Szakács, J.; Váró, G. The Photochemical Reaction Cycle of Proteorhodopsin at Low pH. *Biophys. J.* **2003**, 84, 3252–3256.
- (11) Friedrich, T.; Geibel, S.; Kalmbach, R.; Chizhov, I.; Ataka, K.; Heberle, J.; Engelhard, M.; Bamberg, E. Proteorhodopsin Is a Light-Driven Proton Pump with Variable Vectoriality. *J. Mol. Biol.* **2002**, 321, 821–838.
- (12) Hempelmann, F.; Hölper, S.; Verhoefen, M.-K.; Woerner, A. C.; Köhler, T.; Fiedler, S.-A.; Pfleger, N.; Wachtveitl, J.; Glaubitz, C. His75-Asp97 Cluster in Green Proteorhodopsin. *J. Am. Chem. Soc.* **2011**, *133*, 4645–4654.
- (13) Bergo, V. B.; Sineshchekov, O. A.; Kralj, J. M.; Partha, R.; Spudich, E. N.; Rothschild, K. J.; Spudich, J. L. His-75 in Proteorhodopsin, a Novel Component in Light-Driven Proton Translocation by Primary Pumps. *J. Biol. Chem.* **2009**, 284, 2836—2843.
- (14) Maciejko, J.; Kaur, J.; Becker-Baldus, J.; Glaubitz, C. Photocycle-Dependent Conformational Changes in the Proteorhodopsin Cross-Protomer Asp—His—Trp Triad Revealed by DNP-Enhanced MAS-NMR. *Proc. Natl. Acad. Sci. U. S. A.* **2019**, *116*, 8342—8349.
- (15) Garczarek, F.; Gerwert, K. Functional Waters in Intraprotein Proton Transfer Monitored by FTIR Difference Spectroscopy. *Nature* **2006**, 439, 109–112.
- (16) Shibata, M.; Tanimoto, T.; Kandori, H. Water Molecules in the Schiff Base Region of Bacteriorhodopsin. *J. Am. Chem. Soc.* **2003**, *125*, 13312–13313.
- (17) Saito, K.; Kandori, H.; Ishikita, H. Factors That Differentiate the H-Bond Strengths of Water Near the Schiff Bases in Bacteriorhodopsin and Anabaena Sensory Rhodopsin. *J. Biol. Chem.* **2012**, 287, 34009–34018.
- (18) Hildebrandt, P.; Stockburger, M. Role of Water in Bacteriorhodopsin's Chromophore: Resonance Raman Study. *Biochemistry* **1984**, 23, 5539–5548.
- (19) Wald, G.; Durell, J.; St. George, R. C. C. The Light Reaction in the Bleaching of Rhodopsin. *Science* **1950**, *111*, 179–181.
- (20) Ran, T.; Ozorowski, G.; Gao, Y.; Sineshchekov, O. A.; Wang, W.; Spudich, J. L.; Luecke, H. Cross-Protomer Interaction with the Photoactive Site in Oligomeric Proteorhodopsin Complexes. *Acta Crystallogr., Sect. D: Biol. Crystallogr.* **2013**, *69*, 1965–1980.
- (21) Ikeda, D.; Furutani, Y.; Kandori, H. FTIR Study of the Retinal Schiff Base and Internal Water Molecules of Proteorhodopsin. *Biochemistry* **2007**, *46*, 5365–5373.
- (22) Feng, J.; Mertz, B. Proteorhodopsin Activation Is Modulated by Dynamic Changes in Internal Hydration. *Biochemistry* **2015**, *54*, 7132–7141.

- (23) The PyMOL Molecular Graphics System, version 1.7.0. Schrödinger: LLC, 2014.
- (24) Frisch, M. J.; Trucks, G. W.; Schlegel, H. B.; Scuseria, G. E.; Robb, M. A.; Cheeseman, J. R.; Scalamani, G.; Barone, V.; Petersson, A.; Nakatsuji, H. et al. *Gaussian 09, revision A.1*; Gaussian, Inc.: Wallingford, CT, 2009.
- (25) Cornell, W. D.; Cieplak, P.; Bayly, C. I.; Gould, I. R.; Merz, K. M.; Ferguson, D. M.; Spellmeyer, D. C.; Fox, T.; Caldwell, J. W.; Kollman, P. A. A Second Generation Force Field for the Simulation of Proteins, Nucleic Acids, and Organic Molecules. *J. Am. Chem. Soc.* 1995, 117, 5179–5197.
- (26) Bode, B. M.; Gordon, M. S. MacMolPlt: A Graphical User Interface for GAMESS. J. Mol. Graphics Modell. 1998, 16, 133–138.
- (27) Perdew, J. P.; Ruzsinszky, A.; Tao, J.; Staroverov, V. N.; Scuseria, G. E.; Csonka, G. I. Prescription for the Design and Selection of Density Functional Approximations: More Constraint Satisfaction with Fewer Fits. *J. Chem. Phys.* **2005**, *123*, 062201.
- (28) Santarsiero, B. D.; James, M. N. G.; Mahendran, M.; Childs, R. F. Crystal Structure of N-Methyl-N-Phenylretinal Iminium Perchlorate; a Structural Model for the Bacteriorhodopsin Chromophore. *J. Am. Chem. Soc.* **1990**, *112*, 9416–9418.
- (29) Kralj, J. M.; Bergo, V. B.; Amsden, J. J.; Spudich, E. N.; Spudich, J. L.; Rothschild, K. J. Protonation State of Glu142 Differs in the Green- and Blue-Absorbing Variants of Proteorhodopsin. *Biochemistry* **2008**, *47*, 3447–3453.
- (30) Ozaki, Y.; Kawashima, T.; Abe-Yoshizumi, R.; Kandori, H. A Color-Determining Amino Acid Residue of Proteorhodopsin. *Biochemistry* **2014**, *53*, 6032–6040.
- (31) Hillebrecht, J. R.; Galan, J.; Rangarajan, R.; Ramos, L.; McCleary, K.; Ward, D. E.; Stuart, J. A.; Birge, R. R. Structure, Function, and Wavelength Selection in Blue-Absorbing Proteorhodopsin†. *Biochemistry* **2006**, *45*, 1579–1590.
- (32) Rangarajan, R.; Galan, J. F.; Whited, G.; Birge, R. R. Mechanism of Spectral Tuning in Green-Absorbing Proteorhodopsin. *Biochemistry* **2007**, *46*, 12679–12686.
- (33) Reckel, S.; Gottstein, D.; Stehle, J.; Löhr, F.; Verhoefen, M.-K.; Takeda, M.; Silvers, R.; Kainosho, M.; Glaubitz, C.; Wachtveitl, J.; et al. Solution NMR Structure of Proteorhodopsin. *Angew. Chem., Int. Ed.* **2011**, *50*, 11942–11946.
- (34) Sekharan, S.; Wei, J. N.; Batista, V. S. The Active Site of Melanopsin: The Biological Clock Photoreceptor. *J. Am. Chem. Soc.* **2012**, *134*, 19536–19539.
- (35) Welke, K.; Frähmcke, J. S.; Watanabe, H. C.; Hegemann, P.; Elstner, M. Color Tuning in Binding Pocket Models of the Chlamydomonas-Type Channelrhodopsins. *J. Phys. Chem. B* **2011**, *115*, 15119–15128.
- (36) Hayashi, S.; Ohmine, I. Proton Transfer in Bacteriorhodopsin: Structure, Excitation, IR Spectra, and Potential Energy Surface Analyses by an Ab Initio QM/MM Method. *J. Phys. Chem. B* **2000**, *104*, 10678–10691.
- (37) Wolter, T.; Elstner, M.; Fischer, S.; Smith, J. C.; Bondar, A.-N. Mechanism by Which Untwisting of Retinal Leads to Productive Bacteriorhodopsin Photocycle States. *J. Phys. Chem. B* **2015**, *119*, 2229–2240.
- (38) Bondar, A.-N.; Fischer, S.; Smith, J. C.; Elstner, M.; Suhai, S. Key Role of Electrostatic Interactions in Bacteriorhodopsin Proton Transfer. *J. Am. Chem. Soc.* **2004**, *126*, 14668–14677.
- (39) Allen, F. H.; Harris, S. E.; Taylor, R. Comparison of Conformer Distributions in the Crystalline State with Conformational Energies Calculated by Ab Initio Techniques. *J. Comput.-Aided Mol. Des.* **1996**, 10, 247–254.
- (40) Sekharan, S.; Mooney, V. L.; Rivalta, I.; Kazmi, M. A.; Neitz, M.; Neitz, J.; Sakmar, T. P.; Yan, E. C. Y.; Batista, V. S. Spectral Tuning of Ultraviolet Cone Pigments: An Interhelical Lock Mechanism. J. Am. Chem. Soc. 2013, 135, 19064–19067.
- (41) Sekharan, S.; Weingart, O.; Buss, V. Ground and Excited States of Retinal Schiff Base Chromophores by Multiconfigurational Perturbation Theory. *Biophys. J.* **2006**, *91*, L07–L09.

- (42) Pal, R.; Sekharan, S.; Batista, V. S. Spectral Tuning in Halorhodopsin: The Chloride Pump Photoreceptor. *J. Am. Chem. Soc.* **2013**, *135*, 9624–9627.
- (43) Borin, V. A.; Wiebeler, C.; Schapiro, I. A QM/MM Study of the Initial Excited State Dynamics of Green-Absorbing Proteorhodopsin. *Faraday Discuss.* **2018**, 207, 137.
- (44) Ding, X.; Sun, C.; Cui, H.; Chen, S.; Gao, Y.; Yang, Y.; Wang, J.; He, X.; Iuga, D.; Tian, F.; et al. Functional Roles of Tyrosine 185 during the Bacteriorhodopsin Photocycle as Revealed by in Situ Spectroscopic Studies. *Biochim. Biophys. Acta, Bioenerg.* **2018**, 1859, 1006–1014.
- (45) Fujimoto, K.; Hayashi, S.; Hasegawa, J.-y.; Nakatsuji, H. Theoretical Studies on the Color-Tuning Mechanism in Retinal Proteins. *J. Chem. Theory Comput.* **2007**, *3*, 605–618.
- (46) Bondar, A.-N.; Fischer, S.; Suhai, S.; Smith, J. C. Tuning of Retinal Twisting in Bacteriorhodopsin Controls the Directionality of the Early Photocycle Steps. *J. Phys. Chem. B* **2005**, *109*, 14786–14788.
- (47) Angel, T. E.; Chance, M. R.; Palczewski, K. Conserved Waters Mediate Structural and Functional Activation of Family A (Rhodopsin-like) G Protein-Coupled Receptors. *Proc. Natl. Acad. Sci. U. S. A.* **2009**, *106*, 8555–8560.
- (48) Luecke, H.; Schobert, B.; Richter, H.-T.; Cartailler, J.-P.; Lanyi, J. K. Structure of Bacteriorhodopsin at 1.55 Å Resolution. *J. Mol. Biol.* **1999**, 291, 899–911.
- (49) Kolbe, M.; Besir, H.; Essen, L.-O.; Oesterhelt, D. Structure of the Light-Driven Chloride Pump Halorhodopsin at 1.8 Å Resolution. *Science* **2000**, 288, 1390–1396.
- (50) Luecke, H.; Schobert, B.; Stagno, J.; Imasheva, E. S.; Wang, J. M.; Balashov, S. P.; Lanyi, J. K. Crystallographic Structure of Xanthorhodopsin, the Light-Driven Proton Pump with a Dual Chromophore. *Proc. Natl. Acad. Sci. U. S. A.* **2008**, *105*, 16561–16565.
- (51) Gushchin, I.; Chervakov, P.; Kuzmichev, P.; Popov, A. N.; Round, E.; Borshchevskiy, V.; Ishchenko, A.; Petrovskaya, L.; Chupin, V.; Dolgikh, D. A.; et al. Structural Insights into the Proton Pumping by Unusual Proteorhodopsin from Nonmarine Bacteria. *Proc. Natl. Acad. Sci. U. S. A.* **2013**, *110*, 12631–12636.
- (52) Altoè, P.; Cembran, A.; Olivucci, M.; Garavelli, M. Aborted Double Bicycle-Pedal Isomerization with Hydrogen Bond Breaking Is the Primary Event of Bacteriorhodopsin Proton Pumping. *Proc. Natl. Acad. Sci. U. S. A.* **2010**, *107*, 20172–20177.
- (53) Melaccio, F.; Ferré, N.; Olivucci, M. Quantum Chemical Modeling of Rhodopsin Mutants Displaying Switchable Colors. *Phys. Chem. Chem. Phys.* **2012**, *14*, 12485–12495.
- (54) Schapiro, I.; Ryazantsev, M. N.; Frutos, L. M.; Ferré, N.; Lindh, R.; Olivucci, M. The Ultrafast Photoisomerizations of Rhodopsin and Bathorhodopsin Are Modulated by Bond Length Alternation and HOOP Driven Electronic Effects. *J. Am. Chem. Soc.* **2011**, *133*, 3354–3364.
- (55) Gozem, S.; Luk, H. L.; Schapiro, I.; Olivucci, M. Theory and Simulation of the Ultrafast Double-Bond Isomerization of Biological Chromophores. *Chem. Rev.* **2017**, *117*, 13502–13565.
- (56) Kato, H. E.; Kamiya, M.; Sugo, S.; Ito, J.; Taniguchi, R.; Orito, A.; Hirata, K.; Inutsuka, A.; Yamanaka, A.; Maturana, A. D.; et al. Atomistic Design of Microbial Opsin-Based Blue-Shifted Optogenetics Tools. *Nat. Commun.* **2015**, *6*, 1.
- (57) Ganapathy, S.; Venselaar, H.; Chen, Q.; de Groot, H. J. M.; Hellingwerf, K. J.; de Grip, W. J. Retinal-Based Proton Pumping in the Near Infrared. *J. Am. Chem. Soc.* **2017**, *139*, 2338–2344.
- (58) Ganapathy, S.; Bécheau, O.; Venselaar, H.; Frölich, S.; van der Steen, J. B.; Chen, Q.; Radwan, S.; Lugtenburg, J.; Hellingwerf, K. J.; de Groot, H. J. M.; et al. Modulation of Spectral Properties and Pump Activity of Proteorhodopsins by Retinal Analogues. *Biochem. J.* **2015**, 467. 333–343.
- (59) Hontani, Y.; Ganapathy, S.; Frehan, S.; Kloz, M.; de Grip, W. J.; Kennis, J. T. M. Strong pH-Dependent Near-Infrared Fluorescence in a Microbial Rhodopsin Reconstituted with a Red-Shifting Retinal Analogue. *J. Phys. Chem. Lett.* **2018**, *9*, 6469–6474.